PCSK9 alleviates doxorubicin-induced pyroptosis of cardiomyocytes

CHAOCHU CUI[1*], JINYU ZHAO[1-3*], XIAOQIAN LI[1], SHENGMING HUANG[1,4], GANG LIU[1], XINHUI XU[1], CAN GUO[1], TIESUO ZHAO[5], JIANG DU[6,7], SHIPENG LI[1], XIANWEI WANG[1] and JIANBO YANG[8]

[1]Henan Key Laboratory of Medical Tissue Regeneration, Henan Medical University, Xinxiang, Henan 453003, P.R. China; [2]Shanxi Provincial Center for Upper Gastrointestinal Cancer Research and Clinical Translation, Heping Hospital Affiliated to Changzhi Medical College, Changzhi, Shanxi 046000, P.R. China; [3]Laboratory of Clinical Research Center, Heping Hospital Affiliated to Changzhi Medical College, Changzhi, Shanxi 046000, P.R. China; [4]Department of Neurosurgery, Rudong County Hospital of Traditional Chinese Medicine, Nantong, Jiangsu 226400, P.R. China; [5]Department of Immunology, School of Basic Medical Sciences, Henan Medical University, Xinxiang, Henan 453000, P.R. China; [6]Henan Joint International Research Laboratory of Stem Cell Medicine, School of Medical Engineering, Henan Medical University, Xinxiang, Henan 453003, P.R. China; [7]National Joint Engineering Laboratory of Stem Cells and Biotherapy, Stem Cells and Biotherapy Engineering Research Center of Henan, School of Life Science and Technology, Henan Medical University, Xinxiang, Henan 453003, P.R. China; [8]Teaching Laboratory of Medical Imaging Technology, School of Life Sciences and Technology, Henan Medical University, Xinxiang, Henan 453003, P.R. China

Received January 17, 2026; Accepted May 27, 2026

DOI: 10.3892/mmr.2026.13965

Abstract. Prolonged survival of patients with cancer has increased the need to address chemotherapy-related cardiovascular complications. Doxorubicin (DOX), a widely used anthracycline, is associated with dose-dependent cardiotoxicity, known as DOX-induced cardiotoxicity (DIC), which limits its clinical utility. DOX triggers cardiomyocyte pyroptosis via the NLRP3/caspase-1/gasdermin D pathway, a potential underlying mechanism of DIC. Proprotein convertase subtilisin/kexin type 9 (PCSK9), a key regulator of lipid metabolism and inflammation, has been implicated in NLRP3 inflammasome activation and the progression of cardiovascular diseases; however, its role in DIC remains unclear. The present study demonstrated that DOX downregulates PCSK9 expression in cardiomyocytes in a dose-dependent manner. Through proteomic analysis and PCSK9 knockout cell and mouse models, it was found that the deletion of PCSK9 exacerbated DOX-induced pyroptosis and cardiac dysfunction. These results revealed the protective effect of PCSK9 in DOX-mediated cardiotoxicity and indicated that PCSK9 regulation may provide a new cardioprotective strategy for patients receiving anthracycline chemotherapy.

Correspondence to: Professor Jianbo Yang, Teaching Laboratory of Medical Imaging Technology, School of Life Sciences and Technology, Henan Medical University, 601 Jinsui Avenue, Xinxiang, Henan 453003, P.R. China
E-mail: yangjianbo12@126.com

Professor Xianwei Wang, Henan Key Laboratory of Medical Tissue Regeneration, Henan Medical University, 601 Jinsui Avenue, Xinxiang, Henan 453003, P.R. China
E-mail: wangxianwei1116@126.com

*Contributed equally

Key words: doxorubicin, proprotein convertase subtilisin/kexin type 9, cardiotoxicity, pyroptosis, cancer

Introduction

Doxorubicin (DOX), one of the most widely used anthracycline antibiotics, is typically used to treat various types of cancer such as breast cancer, ovarian cancer and leukemia (1-4). However, its side effects, particularly cardiotoxicity, severely limit its clinical application. The cardiotoxicity induced by DOX involves multiple molecular mechanisms, including redox homeostasis imbalance, DNA and RNA damage, autophagy inhibition and programmed cell death (such as pyroptosis and apoptosis), ultimately leading to myocardial dysfunction (5-7). The dose-dependent cardiotoxicity associated with DOX treatment can eventually develop into congestive heart failure or even death (8,9). Although these mechanisms have been partially elucidated, the corresponding effective clinical intervention measures remain limited, and DOX-induced cardiotoxicity (DIC) has not fundamentally been improved in clinical practice (10). Therefore, further understanding the novel mechanisms underlying DIC is vital for the development of novel cardioprotective strategies.

Proprotein convertase subtilisin/kexin type 9 (PCSK9), a gene typically associated with familial hypercholesterolemia, is expressed predominantly in the liver, kidneys and

intestines (11). PCSK9 affects the level of low-density lipoprotein cholesterol (LDL-C) in the blood by regulating the degradation of LDL receptors (LDLRs) (12). PCSK9 is not only closely associated with cholesterol metabolism but also serves important roles in cardiovascular diseases such as in atherosclerosis and cardiac ischemia-reperfusion injury (13-15). In addition, PCSK9 is involved in various biological processes, such as apoptosis, autophagy, inflammation and tumor immunity, and is closely related to diabetes and neurodegenerative diseases (6,16-19). Recent research has further indicated that PCSK9 also serves a regulatory role in other physiological processes of the heart, including influencing the stress responses and death processes of cardiomyocytes (7,20). The expression levels of LDLR and CD36 are increased and lipids accumulate in the cardiac tissue of PCSK9 knockout mice (21). Clinical studies have demonstrated that elevated expression levels of PCSK9 in peripheral blood are independently associated with increased disease severity and poor prognosis in patients with heart failure (22). These metabolic and functional disturbances suggest PCSK9 dysregulation is closely associated with heart failure. Although the role of PCSK9 in heart diseases has been previously investigated, the specific mechanism through which PCSK9 affects DIC remains unclear. DOX can cause myocardial injury through multiple pathways, including pyroptosis (23). Pyroptosis is a form of lytic cell death mediated by members of the gasdermin protein family that is characterized by cell membrane perforation, cell swelling and rupture, and the release of large amounts of proinflammatory factors (such as IL-1β and IL-18) (24). A study has shown that DOX can trigger pyroptosis (25); however, it is currently unclear whether PCSK9 is involved in this process. Therefore, the present study aimed to explore the regulatory role of PCSK9 in DOX-induced pyroptosis of cardiomyocytes, thereby providing novel insights into reducing cardiotoxicity caused by anthracyclines. These findings offer a new theoretical basis and target for improving the quality of life and therapeutic effect of chemotherapy.

Materials and methods

Cell culture and experimental design. AC-16 cells were provided by the Henan Key Laboratory of Medical Tissue Regeneration of Henan Medical University (Xinxiang, China). The AC-16 cells from the 5th to 8th passages were used in the present study, ensuring stable cell conditions and a consistent phenotype. AC-16 cells were cultured in Dulbecco's Modified Eagle's Medium/F12 (cat. no. 12634010; Gibco; Thermo Fisher Scientific, Inc.) supplemented with 10% fetal bovine serum and 1% penicillin-streptomycin (cat. no. 15070063; Gibco; Thermo Fisher Scientific, Inc.). All cells were cultured at 37˚C with 5% CO_2.

DOX was dissolved in sterile DMSO at a stock concentration of 100 mM and stored at -20˚C. The DOX solution was then diluted directly with culture medium to the working concentration, resulting in a final DMSO concentration <0.001% in all groups. The final working concentration of DOX in the cell culture medium was 0.2 μM, which was consistent with the present IC_{50} results. Control cells received an equal volume of culture medium containing the same concentration of DMSO without DOX.

Animal and experimental design. The present study used two mouse models as follows: Male C57BL/6J mice (age, 6-8 weeks; weight, 18-22 g) and male $PCSK9^{-/-}$ mice (age, 6-8 weeks; weight, 18-22 g) purchased from Shanghai Model Organisms Center. A total of 32 mice (16 male C57BL/6J mice and 16 $PCSK9^{-/-}$ mice) were included in the experiment, and each mouse model was randomly divided into two groups with n=8 mice per group. Grouping was performed using a random number table method to avoid grouping bias by ensuring that the body weight, age and other baseline indicators of the mice in each group were comparable. All the animals were housed under standard laboratory conditions (22±2˚C, 50±5% relative humidity and 12-h light/dark cycle). Food and water were available *ad libitum* throughout the experiment.

The mice were randomly divided into DOX and control groups and subjected to intraperitoneal injections of either DOX (4 mg/kg; cat. no. D107159; Aladdin Scientific Corp.), with an accumulated dosage of 20 mg/kg, or an equivalent volume of saline once per week for five weeks, respectively. This is a common modelling approach for chronic cardiotoxicity; a systematic review has confirmed that a cumulative dose of 15-24 mg/kg reliably induces cardiac injury, and the survival rate at a dose of ≥20 mg/kg is approximately 30% (26).

All animals were monitored twice daily (every 12 h) for signs of pain, distress or impending death. Predefined humane endpoints including weight loss >20%, severe matting of the fur with reduced activity or food intake, dyspnea, inability to reach food or water, and spontaneous recumbency were strictly applied. Animals meeting any endpoint were immediately sacrificed under deep isoflurane anesthesia (inhalation of 5% isoflurane until loss of consciousness and lack of response to toe pinch, 5-10 min) by cervical dislocation. Those exhibiting moderate distress (15-20% weight loss, mild symptoms) received supportive care (subcutaneous fluids, warmth and wet diet) and were re-evaluated after 12-24 h; sacrifice followed if no improvement was observed.

Following the echocardiographic examination, the mice were sacrificed by cervical dislocation performed under deep anesthesia (5% isoflurane for 2-3 min), and the cardiac tissue was rapidly collected for subsequent analysis. All animal procedures were conducted in accordance with animal welfare guidelines and were approved by the Institutional Animal Care and Use Committee of Xinxiang Medical University (currently Henan Medical University; approval no. XYLL-20220192; Xinxiang, China).

Echocardiography. Cardiac function was assessed by echocardiography five weeks after the initiation of the injections. The cardiac function of the mice was evaluated using a high-resolution small animal ultrasound imaging system (Visual Sonics Vevo® 2100; FUJIFILM Corporation). Anesthesia was induced using isoflurane (RWD Life Science Co., Ltd.) at a concentration of 3-4%, with a maintenance concentration of 1.5-2%. Once the required level of anesthesia was confirmed using the toe pinch reflex test, the mice were immobilized in the supine position, with ECG electrodes were attached to their limbs, on a constant-temperature platform (37˚C) to maintain a stable physiological state (37±0.5˚C). Through transthoracic echocardiography, the short-axis section of the left ventricle was located using two-dimensional ultrasound, and the inner

diameters of the left ventricle during systole and diastole were recorded using M-mode ultrasound. The ejection fraction (EF) and left ventricular fractional shortening (FS) were calculated as the core indicators of cardiac function.

Western blotting. AC-16 cells treated with DOX or DMSO for 48 h were lysed on ice in RIPA buffer (cat. no. P0013B; Beyotime Biotechnology) containing PMSF. Protein concentrations were measured by BCA assay. Equal amounts of protein (20 μg per lane) were separated by SDS-PAGE with 10-12% gels and transferred onto PVDF membranes. The membranes were blocked with 5% skimmed milk powder (cat. no. GC310001; Wuhan Servicebio Technology Co., Ltd.) in PBS containing 0.1% Tween-20 (cat. no. P9416; MilliporeSigma) for 1 h and then probed with specific primary antibodies against PCSK9 (1:1,000; cat. no. CY6876; Shanghai Abways Biotechnology Co., Ltd.), IL-1β (1:1,000; cat. no HL1421; Thermo Fisher Scientific, Inc.), caspase-1 (1:1,000; cat. no. 22915-1-AP; Proteintech Group, Inc.), sterol regulatory element binding protein-1 (SREBP-1;1:1,000; cat. no. HA722160; HUABIO), SREBP-2 (1:1,000; cat. no. 28212-1-AP, Proteintech Group, Inc.) and β-actin (1:1,000; cat. no. AB0035; Shanghai Abways Biotechnology Co., Ltd.) overnight at 4˚C. Following primary antibody incubation, the membranes were incubated overnight with the corresponding secondary antibodies Goat anti-rabbit IgG HRP conjugate (1:8,000; cat. no. AB0101 Shanghai Abways Biotechnology Co., Ltd.). Secondary antibody incubation was performed for 1 h at room temperature. Protein signals were visualized using an enhanced chemiluminescence (ECL) kit (cat. no. P0018FS; Beyotime Biotechnology) and imaged with the Amersham™ Imager 600 system (Cytiva). Band intensity was analyzed using ImageJ (version 1.54f, National Institutes of Health, USA) and normalized to β-actin as an internal control.

Reverse transcription-qPCR. Total RNA was extracted from DOX-treated and control AC-16 cells using RNAiso Plus (cat. no. 9108Q; Takara Bio, Inc.) according to the manufacturer's instructions. Total RNA was reverse transcribed to cDNA using PrimerScript RT Master Mix (cat. no. RR036A; Takara Bio, Inc.) according to the manufacturer's instructions, and real-time qPCR was performed using a SYBR Green Kit (cat. no. Q221-01; Vazyme Biotech Co., Ltd.). The thermal cycling conditions were as follows: Initial denaturation at 95˚C for 5 min, followed by 40 cycles of denaturation at 95˚C for 10-15 sec and combined annealing/extension at 60˚C for 30-40 sec. Fluorescence data were collected during the annealing/extension step. Following amplification, a melting curve analysis was performed to verify the specificity of the PCR products. β-actin was used as the control, and the relative expression of the genes was quantified by the $2^{-\Delta\Delta Cq}$ method (27). The primer sequences are listed in Table SI.

Lactate dehydrogenase (LDH) assay. AC-16 cells were seeded in 96-well plates ($1x10^4$ cells/well) and treated with DOX for 48 h. Blank (no cells), negative (untreated) and positive (treated with LDH release reagent) controls groups were also included. After centrifugation at 400 x g for 5 min at room temperature, the supernatant was collected and added to a new 96-well plate, after which the working solution from the LDH Cytotoxicity Assay kit (cat. no. C0017; Beyotime Biotechnology) was added (according to the manufacturer's instructions). The mixture was incubated at room temperature in the dark for 30 min. Absorbance was detected at two wavelengths (main wavelength, 490 nm; reference wavelength, 600 nm) using a microplate reader.

CCK-8 assay. AC-16 cells were seeded into 96-well plates ($5x10^3$ cells/well) and cultured overnight at 37˚C and 5% CO_2. The culture medium was then replaced with fresh medium containing a gradient concentration of DOX (0, 0.1, 0.2, 0.3, 0.4, 0.5 and 0.6 μM), and the cells were further cultured at 37˚C for 24 or 48 h. Subsequently, 10 μl of CCK-8 reagent (cat. no. C0038; Beyotime Biotechnology) was added to each well, and the plates were incubated at 37˚C in the dark for 4 h. The absorbance was detected at 450 nm using a microplate reader.

Immunofluorescence staining. AC-16 cells were seeded onto glass slides in 12-well plates ($5x10^5$ cells/ml) and cultured at 37˚C and 5% CO_2 overnight. Cells were treated with DOX or DMSO for 24 h, washed with PBS, fixed with 4% paraformaldehyde at room temperature for 15 min and permeabilized with 0.3% Triton X-100 for 10 min. The cells were blocked with 5% BSA (cat. no. 9048-46-8; Beijing Solarbio Science & Technology Co., Ltd.) at room temperature for 1 h and incubated overnight at 4˚C with specific primary antibodies against PCSK9 (1:250; cat. no. HA610371; HUABIO), caspase-1 (1:200; cat. no. MA5-16215; Thermo Fisher Scientific, Inc.) and gasdermin D (GSDMD; 1:200; cat. no. PA5-116815; Thermo Fisher Scientific, Inc.). Then, the cells were treated with fluorescent Alexa Fluor 488-conjugated goat anti-rabbit IgG (H+L) (1:500; cat. no. A-11008; Thermo Fisher Scientific, Inc.) and Alexa Fluor 594-conjugated goat anti-mouse IgG (H+L) (1:500; cat. no. A-11005; Thermo Fisher Scientific, Inc.) for 1 h at room temperature in the dark. Finally, nuclear staining was performed with 5 μg/ml DAPI (cat. no. D9542; MilliporeSigma) in PBS at room temperature for 5 min. The cells were observed and images captured using a fluorescence microscope. All images were acquired using the same optimized imaging parameters and were applied uniformly to all samples. Image analysis was performed using ImageJ software (version 1.54f; National Institutes of Health).

Lentiviral packaging and transduction of short hairpin RNA (shRNA) in AC-16 cells. 293 cells (provided by the Henan Key Laboratory of Medical Tissue Regeneration of Henan Medical University, Xinxiang, China) were used for lentiviral packaging. Cells were cultured in DMEM supplemented with 10% fetal bovine serum and 1% penicillin/streptomycin at 37˚C in a 5% CO_2 incubator. 293 cells were co-transfected with either sh-PCSK9 or sh-negative control (NC) plasmids (pLKO.1 vector; cat. no. 12260; Addgene, Inc.), a packaging plasmid (psPAX2; cat. no. 12260; Addgene, Inc.) and an envelope plasmid (pMD2.G; cat. no. 12259; Addgene, Inc.), which together constituted a second-generation lentiviral packaging system.

Transfection was performed using Lipofectamine® 3000 (cat. no. L3000015; Thermo Fisher Scientific, Inc.) according to the manufacturer's protocol. The following amounts of

plasmids were used per 10-cm dish: 5 μg of shRNA plasmid (pLKO.1-sh-PCSK9 or sh-NC), 3.75 μg of psPAX2 and 1.25 μg of pMD2.G (ratio of shRNA: psPAX2: pMD2.G=4:3:1), all diluted in Opti-MEM medium. The DNA-Lipofectamine® 3000 complexes were incubated for 15 min at room temperature before being added to the cells. Viral supernatants were collected at 48 h and 72 h post-transfection, filtered (0.45 μm) and concentrated using a Lenti-X Concentrator (cat. no. 631231; Takara Bio, Inc.) according to the manufacturer's instructions. The concentrated lentiviral pellets were resuspended in 1/100 of the original volume of sterile PBS or culture medium and stored at -80˚C until use. The target sequences were as follows: sh-PCSK9, 5'-GCATGTCTT CCATGGCCTTCT-3'; sh-NC (negative control, scrambled) 5'-TTCTCCGAACGTGTCACGTAA-3'.

AC-16 cells were seeded in 6-well plates ($5\mathbf{x}10^4$ cells/well) and incubated overnight. The cells were then transduced with the concentrated lentivirus (sh-PCSK9 or sh-NC) at a multiplicity of infection (MOI) of 5 in the presence of 5 μg/ml polybrene (cat. no. C0351; Beyotime Biotechnology) at 37˚C for 24 h. After a 48 h recovery period, the cells were selected using 2 μg/ml puromycin (cat. no. ST551; Beyotime Biotechnology) for seven days. Knockdown efficiency was validated by qPCR and western blotting.

Masson's trichrome staining. Heart tissues were fixed in 4% paraformaldehyde (PFA; cat. no. P0099; Beyotime Biotechnology) at 4˚C for 24 h, embedded in paraffin, and cut into 4-μm sections. Sections were stained using a Masson's trichrome kit (cat. no. G1340; Beijing Solarbio Science & Technology Co., Ltd.) according to the manufacturer's protocol. Images were captured using a light microscope (Olympus BX53; Olympus Corporation).

Proteomics analysis. AC-16 cells were divided into two groups: A control group (treated with vehicle alone) and a DOX-treated group (treated with DOX at 1 μM for 48 h). Cells were lysed in RIPA buffer (cat. no. P0013B; Beyotime Biotechnology) containing protease inhibitor cocktail (cat. no. 78430; Thermo Fisher Scientific). Proteins were reduced with 10 mM DTT (cat. no. D0632; MilliporeSigma) at 56˚C for 30 min, alkylated with 20 mM iodoacetamide (cat. no. I1149; MilliporeSigma) in the dark at room temperature for 30 min and then separated by SDS-PAGE (12% gel). After Coomassie Blue staining (cat. no. P0017A; Beyotime Biotechnology) at room temperature for 1 h, the gel lanes were excised and digested overnight with trypsin (cat. no. V5111; Promega Corporation) at 37˚C. The resulting peptides were analyzed by nano-LC-MS/MS using an EASY-nLC 1200 chromatograph coupled to a Q-Exactive HF-X mass spectrometer (Thermo Fisher Scientific). The mass spectrometer was operated in positive ion mode with a spray voltage of 2.1 kV, ion transfer tube temperature of 275˚C, and ion source heater temperature of 300˚C. Sheath and auxiliary gas flows were set to 35 and 10 arbitrary units, respectively. Peptides were separated on a C18 column with a 90-min linear gradient from 3 to 35% acetonitrile in 0.1% formic acid. MS data were acquired in data-dependent mode (scan range m/z 375-1500).

Raw data were processed using the MaxQuant software (version 2.3.1.0; Max Planck Institute of Biochemistry) against the UniProt human database (2023 release; https://www.uniprot.org/). Trypsin was specified as the cleavage enzyme with a maximum of two missed cleavages allowed. Carbamidomethylation of cysteine was set as a fixed modification, and oxidation of methionine and acetylation of the protein N-terminus were set as variable modifications. Protein identification was conducted with a false discovery rate (FDR) <1% at both the peptide and protein levels. Label-free quantification was performed using the MaxQuant software, and proteins with $|\log2(FC)| > 1$ and $P<0.05$ were defined as differentially abundant proteins (DAPs).

DAPs were subjected to gene ontology (GO) and Kyoto Encyclopedia of Genes and Genomes (KEGG) enrichment analyses using DAVID bioinformatics resources (version 6.8; https://david.ncifcrf.gov/). To ensure statistical reliability, significantly enriched GO terms and KEGG pathways were identified using a threshold of $P<0.05$, FDR<0.05, and a minimum gene count of ≥2 per term/pathway. The enrichment results were subsequently used for bioinformatic interpretation and subsequent experimental validation. The sequencing was performed by Novogene (Novogene Co., Ltd.).

Data analysis. The experimental data were analyzed using the GraphPad Prism (version 9.0; Dotmatics) software. An unpaired Student's t-test was used for comparisons between two groups (the data conformed to a normal distribution and were homogeneous), and one-way ANOVA followed by Tukey's post hoc test was used for comparisons among multiple groups. The data are expressed as the mean ± SEM. $P<0.05$ was considered to indicate a statistically significant difference.

Results

DOX treatment downregulates PCSK9 expression and induces cardiomyocyte injury. Compared with those in the control group, cells in the DOX-treated experimental groups showed notable morphological changes including balloon-like transformation and vacuolation, particularly with the increase of DOX concentration at 0.4 μM treatment for 48 h (Fig. 1A). These morphological alterations are consistent with previous reports showing that doxorubicin induces concentration-dependent cytoplasmic vacuolization, nuclear swelling, and mitochondrial disruption in cardiomyocytes (28). CCK-8 results showed that DOX decreased the viability of AC-16 cells in a dose-dependent manner after treatment with DOX at different concentrations for 24 and 48 h, respectively. The semi-inhibitory concentration (IC_{50}) value of DOX for AC-16 cells was 0.2 μM in the 48 h treatment group (Fig. 1B). LDH is a soluble cytoplasmic enzyme; upon cell membrane damage, LDH is released from the cytosol into the culture medium, serving as a well-established biochemical marker of cell death and membrane integrity impairment (29). LDH release was significantly elevated with increasing DOX concentration (Fig. 1C). These results suggested that DOX has a significant damaging effect on cardiomyocytes.

In accordance with the aforementioned experimental results, AC-16 cells were treated with 0.2 μM DOX for 48 h, after which proteomic sequencing was performed, and the results were analyzed. First, principal component analysis was used to reduce the dimensionality of the total

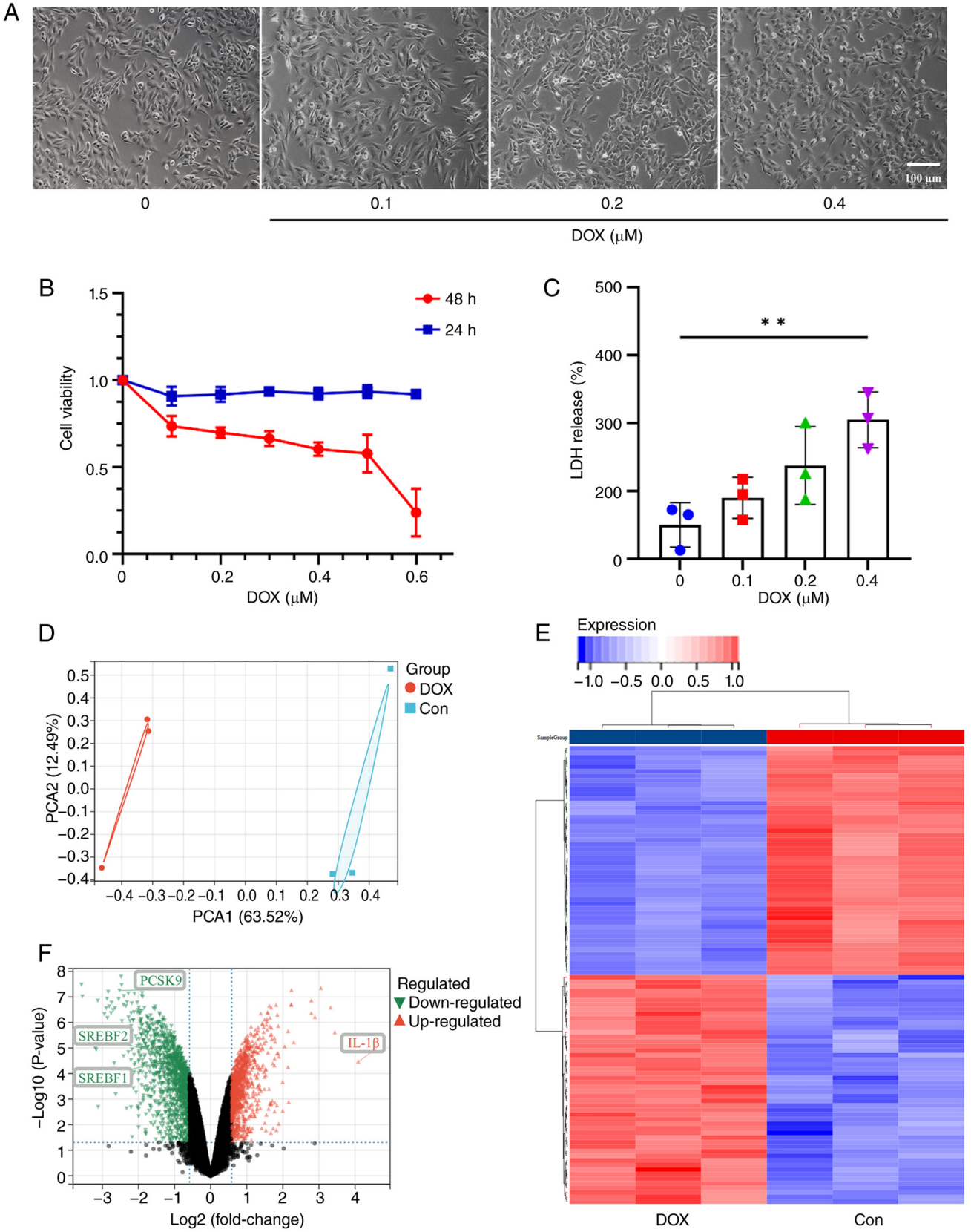

Figure 1. Toxicity and biogenic analysis of DOX in cardiomyocytes. (A) Cell morphology of AC-16 cells under a light microscope after treatment with DOX for 48 h. (B) The cell viability of AC-16 cells after treatment with increasing concentrations of DOX for 24 and 28 h was determined using the Cell Counting Kit-8 assay. (C) LDH release in AC-16 cells treated with different concentrations of DOX for 48 h. (D) PCA revealed a significant difference between the DOX and control group. (E) The heatmap shows the cluster analysis of differentially expressed genes, with different colors representing the level of gene expression. (F) Key genes regulating cholesterol metabolism and lipid synthesis, such as PCSK9, SREBF2 and SREBF1, as well as the important proinflammatory cytokine IL-1β, showed significant changes in abundance (outlined). Red represents upregulated proteins and green represents downregulated proteins and black represents the proteins with no significant changes in expression. The differentially abundant protein volcano plot uses the fold change (log_2) value as the X-axis and the P-value ($-log_{10}$) as the Y-axis. **P<0.01; n=3. DOX, doxorubicin; PCA, principal component analysis; LDH, lactate dehydrogenase; Con, control; PCSK9, Proprotein convertase subtilisin/kexin type 9; SREBF, sterol regulatory element binding transcription factor 2.

protein expression profiles of the experimental and control groups. PCA analysis demonstrated a significant difference between the DOX and control groups (Fig. 1D). Heatmap analysis also revealed significant differences in protein levels between the DOX-treated and control group (Fig. 1E). To further elucidate the potential mechanisms underlying DOX-induced myocardial injury, an in-depth analysis based on the results of proteomic KEGG enrichment analysis was conducted (Fig. S1). The results showed that differentially expressed proteins were significantly enriched in several core lipid metabolic pathways, including 'steroid metabolism', 'sterol metabolism', 'cholesterol metabolism' and 'lipid storage regulation'. This finding suggested that DOX-induced myocardial injury is closely associated with disrupted lipid homeostasis, and that PCSK9 may participate in this pathological process by regulating lipid metabolism via the classical LDLR pathway. Furthermore, proteomic results revealed a significant enrichment of differentially expressed proteins in inflammation- and stress-related pathways (such as 'starvation response' and 'Notch signaling pathway'). This suggested that PCSK9 may also possess non-classical functions independent of lipid metabolism, such as the direct regulation of inflammatory or stress signaling pathways.

Furthermore, statistical analysis of the proteomics data was conducted using a two-tailed independent sample t-test, and fold-change>1.2 and FDR<0.05 were set as screening thresholds to define differentially expressed proteins. Compared with the control group, the expression levels SREBF/SREBP-1, SREBF-2/SREBP-2 and PCSK9, key genes associated with lipid metabolism, were significantly downregulated in the DOX-treated group (Fig. 1F). IL-1β, which is closely related to inflammation and pyrosis expression, was upregulated in the DOX-treated group compared with the control group. Among these differentially expressed genes, PCSK9 was selected for further investigation due to its central role in lipid metabolism and its emerging regulatory functions in inflammatory responses and cardiomyocyte injury. Moreover, recent studies have suggested a potential crosstalk between PCSK9 and IL-1β-mediated signaling pathways, although direct evidence in the context of doxorubicin-induced cardiotoxicity remains limited. Based on these correlative observations, it is plausible that PCSK9 may be involved in IL-1β-mediated myocardial cell injury, but further mechanistic studies are required to establish a causal relationship.

PCSK9 expression in DOX-induced cardiomyocyte pyroptosis. Further verification of the proteomics results by immunofluorescence, qPCR and western blotting demonstrated that DOX significantly reduced PCSK9 expression at both the mRNA and protein levels in a dose-dependent manner (Fig. 2A-E). The proteomics analysis initially identified IL-1β as a differentially expressed protein associated with inflammation. The present study further evaluated additional key pyroptosis-related markers including caspase-1, GSDMD and NLRP3, based on their established roles as core components of the canonical pyroptosis pathway downstream of IL-1β signaling. Specifically, NLRP3 functions as an upstream inflammasome sensor, caspase-1 serves as the executioner protease that cleaves pro-IL-1β and pro-IL-18, and GSDMD is the pore-forming effector that mediates membrane rupture and pyroptotic cell death (30,31). Therefore, these molecules were selected to comprehensively assess whether DOX induces pyroptosis in AC-16 cells. In accordance with the proteomic sequencing results, AC-16 cells were treated with different concentrations of DOX, and the mRNA expression levels of IL-1β, caspase-1, GSDMD and NLRP3 were determined. The mRNA expression levels of these genes increased in a dose-dependent manner (Fig. 2F-I). Furthermore, the protein expression levels of IL-1β and caspase-1 were determined by using western blotting. The protein expression levels of IL-1β and caspase-1 were significantly increased in AC-16 cells after treatment with 0.2 μM DOX for 48 h, compared with that of control cells (Fig. 2J-L).

Intervention with PCSK9 expression alleviates DOX-induced pyroptosis. To explore the relationship between PCSK9- and DOX-induced pyroptosis in cardiomyocytes, PCSK9-knockdown AC-16 cells were constructed by lentivirus transfection with shRNA targeting the PCSK9 gene. The knockdown effect was verified by determining PCSK9 mRNA and protein expression in cells. The transcription and protein levels of PCSK9 were significantly decreased in sh-PCK9 cells compared with control cells (Fig. 3A-E). The mRNA expression levels of IL-1β, caspase-1, GSDMD and NLRP3 were markedly increased in the sh-PCSK9 group compared with those in the sh-NC group, and the increase was even more pronounced in the sh-PCSK9+DOX group compared with the sh-NC+DOX group (Fig. 3F-I). Furthermore, the protein expression levels of IL-1β were consistent with the changes in mRNA expression in sh-PCSK9+DOX cells compared with sh-NC+DOX cells (Fig. 3J-K). These results suggested that knockdown of PCSK9 can exacerbate the increase in myocardial pyroptosis induced by DOX.

PCSK9 knockout reduced the tolerance of mice to DOX. The *in vivo* effects of the present cell experiments were further verified using PCSK9 knockout transgenic mice. Mouse tail genotype identification demonstrated that WT mice presented a single target band (568 bp), whereas $PCSK9^{-/-}$ mice presented a mutant band (837 bp) (Fig. 4A). By the 30th day of modeling, the survival rate of the WT mice decreased, and the survival rate of the $PCSK9^{-/-}$ mice decreased markedly by >50% (Fig. 4B). Compared with the control group, the mice in DOX modeling group showed dull hair, slow movement and weight loss (Fig. 4C). Masson's trichrome staining revealed that compared with those in the WT group, the mice in the WT DOX group showed obvious fibrosis within the myocardium (Fig. 4D). Moreover, PCSK9-deficient mice exhibited more severe cardiac fibrosis upon DOX challenge, as evidenced by the increased collagen deposition in the $PCSK9^{-/-}$ DOX group compared with the WT DOX group (Fig. 4D).

EF and FS are two important parameters commonly used in echocardiography to evaluate the systolic function of the heart (9). Compared with those in the WT group, the EF and FS were decreased in the WT DOX group and were further reduced in the $PCSK9^{-/-}$ DOX group (Fig. 4E-G). Consistent with the functional deterioration observed in echocardiography, PCSK9 deficiency exacerbated DOX-induced

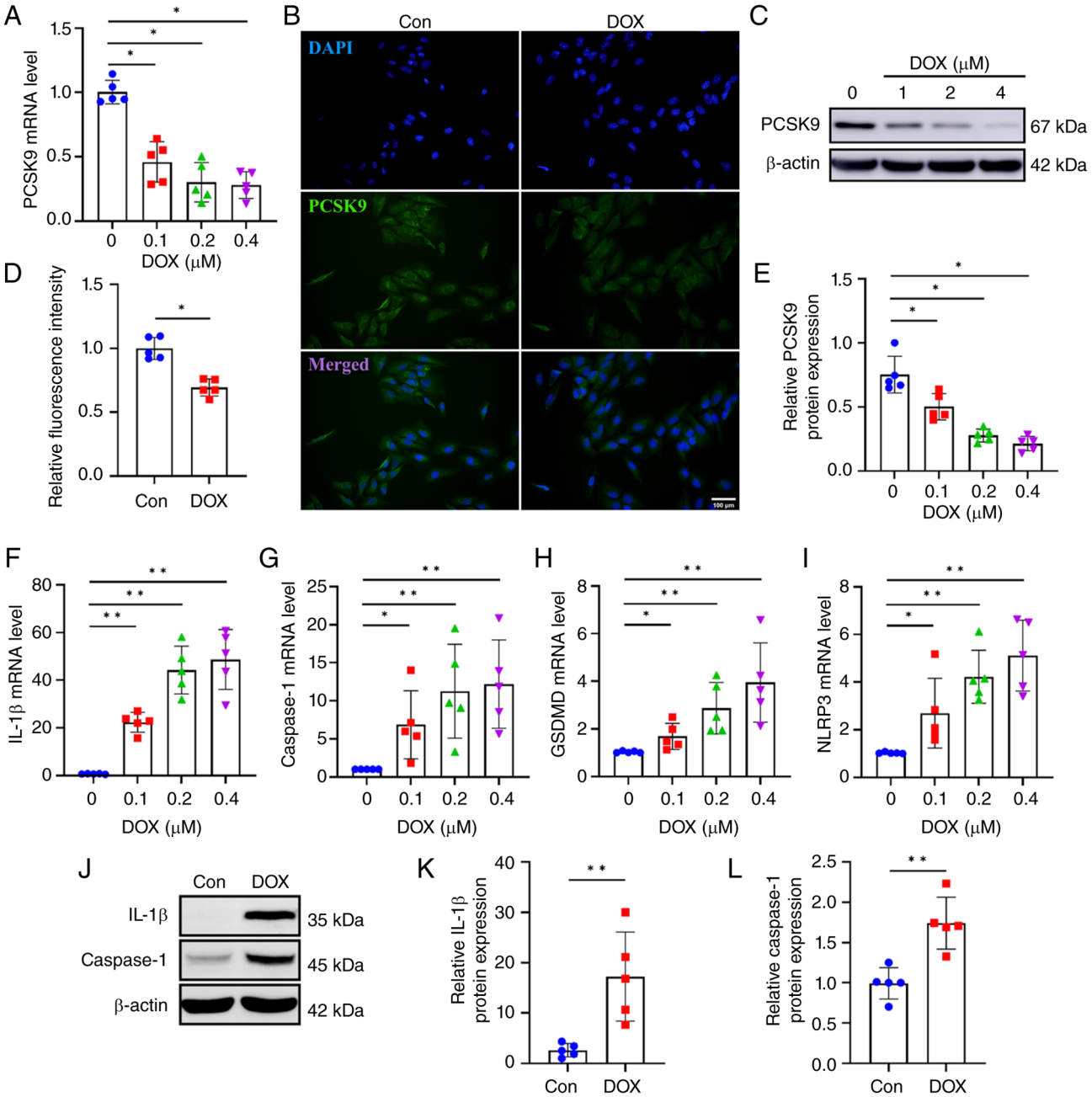

Figure 2. Decreased expression levels of PCSK9 in DOX-induced cardiomyocyte pyroptosis. (A) The expression of PCSK9 mRNA was detected using qPCR. Immunofluorescence labeling of PCSK9 (B) subcellular localization and (D) quantitative analysis of fluorescence intensity (scale bar, 100 μm). (C) Representative western blot images and (E) quantification of PCSK9 protein expression levels. The expression levels of (F) IL-1β, (G) caspase-1, (H) GSDMD and (I) NLRP3 mRNA were detected by qPCR. (J) Representative western blot images and quantification of (K) IL-1β and (L) caspase-1 protein expression levels. *P<0.05; **P<0.01. n=5. DOX, doxorubicin; PCSK9, Proprotein convertase subtilisin/kexin type 9; GSDMD, gasdermin D, NLRP3, NOD-, LRR- and pyrin domain-containing protein 3.

cardiac systolic dysfunction, leading to a more pronounced decline in both ejection fraction and fractional shortening. Compared with the WT group, the protein expression levels of GSDMD and caspase-1 in the heart tissues of DOX-treated WT mice (WT DOX group) were markedly elevated, but a notably greater increase was observed in the PCSK9$^{-/-}$ DOX mice compared with the WT DOX group (Fig. 4H). These results suggested that PCSK9 knockout renders mice less tolerant to DOX-induced myocardial damage, possibly by exacerbating pyroptosis-related inflammatory responses and cardiac fibrosis.

Discussion

In current clinical practice, the cardiotoxicity induced by chemotherapeutic agents remains an unavoidable and challenging issue to address (32). DOX is a widely used anthracycline chemotherapy drug (1). Although the use of DOX has shown significant efficacy in antitumor treatment, its clinical application is considerably restricted by notable cardiotoxic reactions (33). In the present study, DOX was used as a representative chemotherapeutic drug to establish a cell and animal model of DOX-induced cardiomyocyte injury, and

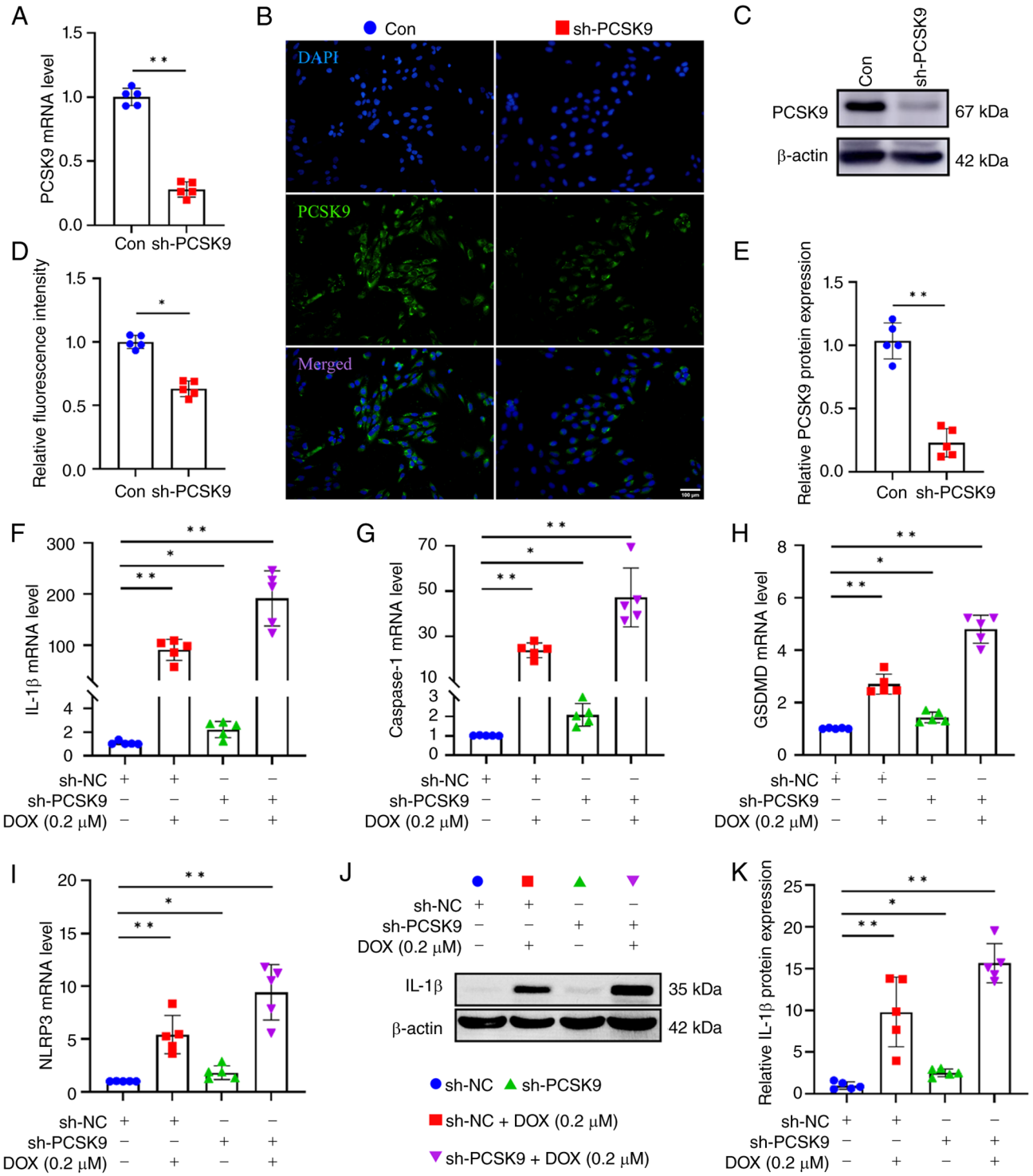

Figure 3. Effects of PCSK9 on DOX-induced AC-16 cell pyroptosis. (A) mRNA expression of PCSK9. (B) Representative immunofluorescence images of PCSK9 subcellular localization (scale bar, 100 μm) and (D) Quantitative analysis of fluorescence intensity. (C) Representative western blot images and (E) quantification of PCSK9 protein expression levels. The mRNA expression levels of (F) IL-1β, (G) caspase-1, (H) GSDMD and (I) NLRP3 were detected using qPCR. (J) Western blotting was used to measure the expression and (K) quantification of IL-1β in AC-16 cells with PCSK9 knockdown. *P<0.05; **P<0.01. n=5. DOX, doxorubicin; PCSK9, Proprotein convertase subtilisin/kexin type 9; GSDMD, gasdermin D, NLRP3, NOD-, LRR- and pyrin domain-containing protein 3.

to further investigate the roles of PCSK9 in DIC. The present results demonstrated that targeting PCSK9 could effectively alleviate DOX-induced cardiomyocyte pyroptosis and cardiac dysfunction.

It was found that DOX treatment significantly reduced the viability of cardiomyocytes, and the cells underwent obvious morphological changes, including balloon-like swelling and vacuolar damage. A previous study has shown that DOX induces cardiotoxicity through a variety of complex and inter-related mechanisms (34). The classic pathway involves the production of a large amount of reactive oxygen species (ROS), leading to oxidative stress damage within cardiomyocytes,

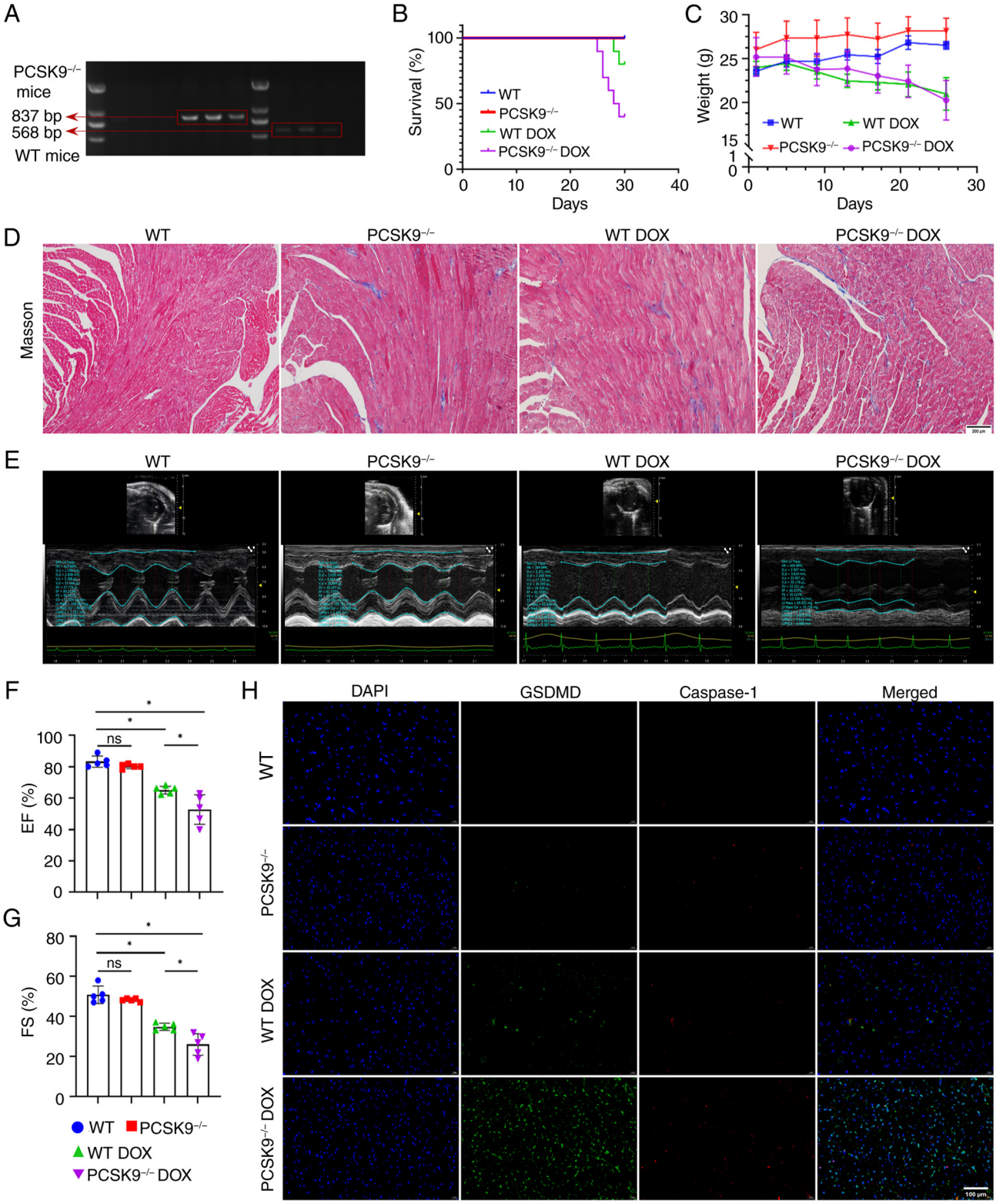

Figure 4. Reduced tolerance to DOX in PCSK9$^{-/-}$ mice. (A) Mouse tail genotype identification of PCSK9$^{-/-}$ mice and WT mice. (B) Changes in the survival rate of mice from the initiation of treatment to Day 30. n=8. (C) Changes in weight of the mice during drug administration. n=8. (D) Masson's trichrome staining was used to evaluate the degree of cardiac fibrosis in the mice (scale bar, 200 μm). (E) The cardiac function of the mice was assessed using echocardiography 25 days after DOX administration. n=5. Assessment of cardiac function in mice: (F) EF and (G) FS. (H) Representative immunofluorescence images of GSDMD and caspase-1 subcellular localization (scale bar, 100 μm). *P<0.05. DOX, doxorubicin; PCSK9, Proprotein convertase subtilisin/kexin type 9; EF, ejection fraction; FS, fractional shortening; GSDMD, gasdermin D.

which triggers DNA damage, lipid peroxidation and mitochondrial dysfunction (35). In addition to oxidative stress, DOX can directly induce apoptosis, necrosis and inflammatory responses in cardiomyocytes and can interfere with the transcription and repair processes of cardiomyocytes by inhibiting topoisomerase IIβ (36-38). In recent years, a study on the

DIC have gradually shifted from traditional mechanisms of oxidative stress and apoptosis to more complex forms of cell death, such as pyroptosis (39). As a form of inflammatory cell death, pyroptosis is characterized by the loss of membrane integrity, cell swelling and the release of inflammatory factors such as IL-1β and IL-18 (40). The present study found that DOX could induce pyroptosis in AC-16 cardiomyocytes in a dose-dependent manner, which is consistent with the findings of previous studies (25,41,42). These multilevel toxicity mechanisms ultimately cause cardiomyocyte death, cardiac function decline and potentially irreversible heart failure.

Proteomic sequencing revealed that the expression of SREBF and PCSK9, which are related to lipid metabolism, was downregulated in cardiomyocytes treated with DOX. In recent years, the role of PCSK9 in cardiovascular diseases has attracted increasing attention (43). Accumulating evidence has demonstrated that PCSK9 exerts context-dependent dual effects on the cardiovascular system, which are closely associated with experimental models, stimulating factors, protein concentration, and the pathophysiological status of the body. Several clinical and basic studies have demonstrated that PCSK9 promotes the development of atherosclerosis via classic lipid metabolic pathways (20,21,44,45). Inhibiting PCSK9 expression or activity effectively reduces circulating lipid levels and decreases the risk of coronary heart disease and major adverse cardiovascular events, providing a rationale for the clinical application of PCSK9 inhibitors in lipid management (46).

A previous study reported that the levels of PCSK9 in the serum and hearts of mice with ischemia-reperfusion injury and in the serum of patients with myocardial infarction are elevated (47). Notably, excessive PCSK9 expression significantly aggravates myocardial remodeling and accelerates the progression of heart failure, indicating that PCSK9 serves a detrimental role in patients with myocardial injury under pathological conditions such as chronic stress (48). Mechanistically, PCSK9 promotes myocardial fibrosis and cardiac remodeling by activating the TLR4/NF-κB/NLRP3 inflammatory signaling pathway and facilitating the proliferation and excessive collagen deposition of cardiac fibroblasts. Furthermore, PCSK9 also facilitates the fibrotic process via the TGF-β1/Smad3 pathway, thereby further impairing cardiac function (48,49).

PCSK9 can also exert noncanonical cardioprotective effects within the myocardial microenvironment, in contrast to its primarily atherogenic role in peripheral blood vessels. A recent study confirmed that cardiomyocyte-specific PCSK9 deficiency leads directly to abnormalities in the assembly and function of mitochondrial respiratory chain complexes. This results in reduced ATP production and increased ROS generation. It also triggers a shift in myocardial metabolism toward glycolysis, as well as cardiac hypertrophy, fibrosis and impaired cardiac function (20). Whole-body PCSK9 knockout leads to reprogrammed myocardial lipid metabolism, mitochondrial dysfunction and abnormal accumulation of lipid droplets. This ultimately results in heart failure with a preserved EF (21).

In the present study, the expression of PCSK9 decreased after cardiomyocytes were treated with DOX. These findings reflect the discourse previously noted clinical research; although PCSK9 inhibitors are widely used to treat hypercholesterolemia, their role in cardiomyo-protection remains controversial. Studies have shown that PCSK9 inhibitors can reduce myocardial damage by lowering cholesterol levels and inhibiting inflammatory responses (47), whereas PCSK9 inhibitors may increase the risk of cardiovascular events while lowering cholesterol levels (50). Therefore, the role of PCSK9 in myocardial protection may be pleiotropic. PCSK9 protects cardiomyocytes by regulating cholesterol metabolism and inhibiting the inflammatory response; conversely, excessive inhibition of PCSK9 may aggravate myocardial injury. However, how PCSK9 regulates this process in the case of anthracycline-induced cardiomyocyte death remains unclear.

Proteomic sequencing of cardiomyocytes treated with DOX also revealed that the expression of IL-1β, which is related to pyroptosis, was upregulated. Therefore, it was speculated that PCSK9 may cause myocardial injury through IL-1β mediated pyroptosis of myocardial cells. To further verify the role of PCSK9 in DIC, models of AC-16 cells with reduced expression of PCSK9 and mice with PCSK9 gene knockout were established. The results showed that PCSK9 deficiency or deletion significantly aggravated DOX-induced myocardial injury, as indicated by increased cardiomyocyte pyroptosis and further deterioration of cardiac function.

A limitation of the present study is the lack of rescue experiments (such as PCSK9 replenishment in PCSK9$^{-/-}$ mice). However, the present loss-of-function data from both *in vitro* knockdown and *in vivo* knockout consistently demonstrated the protective role of endogenous PCSK9 against DOX-induced pyroptosis and cardiac dysfunction. DOX significantly downregulated the expression level of PCSK9 in AC-16 cells in a dose-dependent manner. By using an *in vitro* cardiomyocyte model and an *in vivo* PCSK9 gene knockout mouse model, it was verified that PCSK9 deletion aggravated myocardial pyroptosis induced by DOX, emphasizing the important role of PCSK9 in myocardial protection, and the specific regulatory molecular mechanisms need to be further studied. The results of the present study provided a novel perspective on the mechanism of the DIC.

Based on these findings, the present study revealed the protective role of PCSK9 in DIC. These results may have considerable translational value and clinical implications; these findings suggest that maintaining or moderately increasing the expression or function of PCSK9 could be a new cardioprotective strategy. In patients with cancer receiving anthracycline-based chemotherapy, maintaining steady-state levels of PCSK9 in cardiomyocytes during treatment may effectively reduce the incidence of myocardial pyroptosis, delaying or even preventing the onset of cardiac dysfunction and heart failure. Furthermore, significant changes in PCSK9 expression levels during myocardial injury suggested that PCSK9 may serve as a potential biomarker for the early identification of individuals at high risk of anthracycline-induced cardiotoxicity. Patients with low baseline PCSK9 levels or a significant decrease in PCSK9 levels during chemotherapy should undergo more frequent cardiac function monitoring and receive cardioprotective interventions early if necessary.

Acknowledgements

Not applicable.

Funding

The present study was sponsored by the Natural Science Foundation of Henan (grant no. 202300410309), the National Natural Science Foundation of China (grant no. 81902442), the Henan Medical University Grant (grant no. XYBSKYZZ201828) and the Graduate Education Reform Project of Henan Province (grant no. 2025SJGLX441Y).

Availability of data and materials

The mass spectrometry proteomics data generated in the present study may be found in the ProteomeXchange Consortium via the iProX partner repository (https://www.iprox.cn) under accession number PXD077062 or at the following URL: https://www.iprox.cn//page/project.html?id=IPX0016598000. All other data generated in the present study may be requested from the corresponding author.

Authors' contributions

CC and JZ conceived and designed the study. SH, XL, GL, XX, CG and SL performed experiments and data analysis. XL conducted a comprehensive secondary review of the manuscript and participated in the supplementary experiments during the revision process. JD provided critical reagents and participated in the interpretation of western blotting and qPCR data. TZ contributed to the interpretation of immunofluorescence staining and western blotting results. XW contributed to the analysis of echocardiography parameters (EF/FS) and data interpretation. JY contributed to the interpretation of pyroptosis-related protein expression data and made critical revisions to the manuscript for important intellectual content. TZ, XW and JY supervised the project and revised the manuscript. CC and JY confirm the authenticity of all the raw data. All authors read and approved of the final manuscript.

Ethics approval and consent to participate

The present study was conducted with ethics approval from the Ethics Committee of Xinxiang Medical University (currently Henan Medical University; approval no. XYLL-20220192; Xinxiang, China).

Patient consent for publication

Not applicable.

Competing interests

The authors declare that they have no competing interests.

References

1. Gergely S, Hegedűs C, Lakatos P, Kovács K, Gáspár R, Csont T and Virág L: High throughput screening identifies a novel compound protecting cardiomyocytes from doxorubicin-induced damage. Oxid Med Cell Longev 2015: 178513, 2015.
2. Bisht A, Avinash D, Sahu KK, Patel P, Das Gupta G and Kurmi BD: A comprehensive review on doxorubicin: Mechanisms, toxicity, clinical trials, combination therapies and nanoformulations in breast cancer. Drug Deliv Transl Res 15: 102-133, 2025.
3. Newhouse R, Nelissen E, El-Shakankery KH, Rogozińska E, Bain E, Veiga S and Morrison J: Pegylated liposomal doxorubicin for relapsed epithelial ovarian cancer. Cochrane Database Syst Rev 7: CD006910, 2023.
4. Zeng Y, Zhang X, Lin D, Feng X, Liu Y, Fang Z, Zhang W, Chen Y, Zhao M, Wu J and Jiang L: A lysosome-targeted dextran-doxorubicin nanodrug overcomes doxorubicin-induced chemoresistance of myeloid leukemia. J Hematol Oncol 14: 189, 2021.
5. Abdel-Daim MM, Kilany OE, Khalifa HA and Ahmed AAM: Allicin ameliorates doxorubicin-induced cardiotoxicity in rats via suppression of oxidative stress, inflammation and apoptosis. Cancer Chemother Pharmacol 80: 745-753, 2017.
6. Xu R, Li T, Luo J, Zhang X, Wang T, Wang Y, Ma Y, Yang B, Jia J, Dmytriw AA, *et al*: PCSK9 increases vulnerability of carotid plaque by promoting mitochondrial dysfunction and apoptosis of vascular smooth muscle cells. CNS Neurosci Ther 30: e14640, 2024.
7. D'Onofrio N, Prattichizzo F, Marfella R, Sardu C, Martino E, Scisciola L, Marfella L, Grotta R, Frige C, Paolisso G, *et al*: SIRT3 mediates the effects of PCSK9 inhibitors on inflammation, autophagy, and oxidative stress in endothelial cells. Theranostics 13: 531-542, 2023.
8. Hamo CE, Bloom MW, Cardinale D, Ky B, Nohria A, Baer L, Skopicki H, Lenihan DJ, Gheorghiade M, Lyon AR and Butler J: Cancer Therapy-related cardiac dysfunction and heart failure: Part 2: Prevention, treatment, guidelines, and future directions. Circ Heart Fail 9: e002843, 2016.
9. Antonini-Canterin F, Pavan D and Nicolosi GL: Echocardiographic evaluation of the volumes and global systolic function of the left ventricle. Ital Heart J Suppl 1: 1261-1272, 2000 (In Italian).
10. Sperling W and Rafferty CN: Relationship between absorption spectrum and molecular conformations of 11-cis-retinal. Nature 224: 590-594, 1969.
11. Seidah NG, Benjannet S, Wickham L, Marcinkiewicz J, Jasmin SB, Stifani S, Basak A, Prat A and Chretien M: The secretory proprotein convertase neural apoptosis-regulated convertase 1 (NARC-1): Liver regeneration and neuronal differentiation. Proc Natl Acad Sci USA 100: 928-933, 2003.
12. Tremblay F, Xiong Q, Shah SS, Ko CW, Kelly K, Morrison MS, Giancarlo C, Ramirez RN, Hildebrand EM, Voytek SB, *et al*: A potent epigenetic editor targeting human PCSK9 for durable reduction of low-density lipoprotein cholesterol levels. Nat Med 31: 1329-1338, 2025.
13. Dogan Z, Senyigit A, Durmus S, Duvarcı C, Gelişgen R, Uzun H and Tabak O: The relationship between oxLDL, sLOX-1, PCSK9 and carotid intima-media thickness in patients with prediabetes and type 2 diabetes. Sci Rep 15: 4554, 2025.
14. Li Z, Zhu L, Xu Y, Zhang Y, Liu Y, Sun H, Li S, Wang M, Jiang T, Zhou J and Deng Q: Pleiotropic effects of PCSK9 inhibitors on Cardio-cerebrovascular diseases. Biomedicines 12: 2729, 2024.
15. Liu G, Yu X, Cui C, Li X, Wang T, Palade PT, Mehta JL and Wang X: The pleiotropic effects of PCSK9 in cardiovascular diseases beyond cholesterol metabolism. Acta Physiol (Oxf) 241: e14272, 2025.
16. Cui C, Yan A, Huang S, Chen Y, Zhao J, Li C, Wang X and Yang J: PCSK9 manipulates lipid metabolism and the immune microenvironment in cancer. Onco Targets Ther 18: 411-427, 2025.
17. Gu Y, Lin X, Dong Y, Wood G, Seidah NG, Werstuck G, Major P, Bonert M, Kapoor A and Tang D PCSK9 facilitates melanoma pathogenesis via a network regulating tumor immunity. J Exp Clin Cancer Res 42: 2, 2023.
18. Gao JJ, Wu FY, Liu YJ, Li L, Lin YJ, Kang YT, Peng YM, Liu YF, Wang C, Ma ZS, *et al*: Increase of PCSK9 expression in diabetes promotes VEGFR2 ubiquitination to inhibit endothelial function and skin wound healing. Sci China Life Sci 67: 2635-2649, 2024.
19. Vilella A, Bodria M, Papotti B, Zanotti I, Zimetti F, Remaggi G, Elviri L, Poti F, Ferri N, Lupo MG, *et al*: PCSK9 ablation attenuates Aβ pathology, neuroinflammation and cognitive dysfunctions in 5XFAD mice. Brain Behav Immun 115: 517-534, 2024.
20. Laudette M, Lindbom M, Arif M, Cinato M, Ruiz M, Doran S, Miljanovic A, Rutberg M, Andersson L, Klevstig M, *et al*: Cardiomyocyte-specific PCSK9 deficiency compromises mitochondrial bioenergetics and heart function. Cardiovasc Res 119: 1537-1552, 2023.

21. Da Dalt L, Castiglioni L, Baragetti A, Audano M, Svecla M, Bonacina F, Pedretti S, Uboldi P, Benzoni P, Giannetti F, *et al*: PCSK9 deficiency rewires heart metabolism and drives heart failure with preserved ejection fraction. Eur Heart J 42: 3078-3090, 2021.
22. Xu Q, Zhao YM, He NQ, Gao R, Xu WX, Zhuo XJ, Ren Z, Wu CY and Liu LS: PCSK9: A emerging participant in heart failure. Biomed Pharmacother 158: 114106, 2023.
23. Fang G, Li X, Yang F, Huang T, Qiu C, Peng K, Wang Z, Yang Y and Lan C: Amentoflavone mitigates doxorubicin-induced cardiotoxicity by suppressing cardiomyocyte pyroptosis and inflammation through inhibition of the STING/NLRP3 signalling pathway. Phytomedicine 117: 154922, 2023.
24. Zhu C, Xu S, Jiang R, Yu Y, Bian J and Zou Z: The gasdermin family: Emerging therapeutic targets in diseases. Signal Transduct Target Ther 9: 87, 2024.
25. Zhang L, Jiang YH, Fan C, Zhang Q, Jiang YH, Li Y and Xue YT: MCC950 attenuates doxorubicin-induced myocardial injury in vivo and in vitro by inhibiting NLRP3-mediated pyroptosis. Biomed Pharmacother 143: 112133, 2021.
26. Li M, Zhang Y, Wu B, Qiu R, Zhao C, Chen B and Shang H: Optimizing dose selection for doxorubicin-induced cardiotoxicity in mice: A comprehensive analysis of single and multiple-dose regimens. Eur J Pharmacol 1003: 177883, 2025.
27. Livak KJ and Schmittgen TD: Analysis of relative gene expression data using real-time quantitative PCR and the 2(-Delta Delta C(T)) method. Methods 25: 402-408, 2001.
28. Sardão VA, Oliveira PJ, Holy J, Oliveira CR and Wallace KB: Morphological alterations induced by doxorubicin on H9c2 myoblasts: Nuclear, mitochondrial, and cytoskeletal targets. Cell Biol Toxicol 25: 227-243, 2009.
29. Méry B, Guy JB, Vallard A, Espenel S, Ardail D, Rodriguez-Lafrasse C, Rancoule C and Magné N: In vitro cell death determination for drug discovery: A landscape review of real issues. J Cell Death 10: 1179670717691251, 2017.
30. Vande Walle L and Lamkanfi M: Drugging the NLRP3 inflammasome: From signalling mechanisms to therapeutic targets. Nat Rev Drug Discov 23: 43-66, 2024.
31. Man SM and Kanneganti TD: Converging roles of caspases in inflammasome activation, cell death and innate immunity. Nat Rev Immunol 16: 7-21, 2016.
32. Madrigal-Burgaleta R, Banerji A, Vazquez-Revuelta P and Guyer AC: New approaches to chemotherapeutic drug allergy: From drug challenge to desensitization. J Allergy Clin Immunol Pract 13: 955-966, 2025.
33. Dempke WCM, Zielinski R, Winkler C, Silberman S, Reuther S and Priebe W: Anthracycline-induced cardiotoxicity-are we about to clear this hurdle? Eur J Cancer 185: 94-104, 2023.
34. Kciuk M, Gielecinska A, Mujwar S, Kolat D, Kaluzinska-Kolat Z, Celik I and Kontek R: Doxorubicin-An agent with multiple mechanisms of anticancer activity. Cells 12: 659, 2023.
35. Hu Y, Yu J, He W, Qiao Y, Cheng X, Huang H, Lai S, Yin D and He H: Astragaloside IV intervenes multi-regulatory cell death forms against doxorubicin-induced cardiotoxicity by regulating AMPKα2 pathway. Int Immunopharmacol 142: 113078, 2024.
36. Tian W, Zhang P, Yang L, Song P, Zhao J, Wang H, Zhao Y and Cao L: Astragaloside IV alleviates Doxorubicin-Induced cardiotoxicity by inhibiting cardiomyocyte pyroptosis through the SIRT1/NLRP3 Pathway. Am J Chin Med 52: 453-469, 2024.
37. Ipek E and Tunca R: Silymarin protects against doxorubicin induced cardiotoxicity by down-regulating topoisomerase IIbeta expression in mice. Biotech Histochem 98: 412-423, 2023.
38. Yu J, Qi HL, Zhang H, Zhao ZY, Jing Z and Nie ZY: Morin inhibits Dox-induced vascular inflammation by regulating PTEN/AKT/NF-κB pathway. Inflammation 45: 2406-2418, 2022.
39. Zhang W, Wang X, Tang Y and Huang C: Melatonin alleviates doxorubicin-induced cardiotoxicity via inhibiting oxidative stress, pyroptosis and apoptosis by activating Sirt1/Nrf2 pathway. Biomed Pharmacother 162: 114591, 2023.
40. Dai S, Chen Y, Fan X, Han J, Zhong L, Zhang Y, Liu Q, Lin J, Huang W, Su L, *et al*: Emodin attenuates cardiomyocyte pyroptosis in doxorubicin-induced cardiotoxicity by directly binding to GSDMD. Phytomedicine 121: 155105, 2023.
41. Chen XT, Yu YH, Du YH, Xu L and Meng XP: MiR-145-5p attenuates Doxorubicin-induced heart injury through targeting cardiomyocyte pyroptosis. Kaohsiung J Med Sci 42: e70126, 2026.
42. Huang X, Chen Y, Zhang Y, Hu X, Yang W, Pan T, Gao W, Eom K, Chen P, Dong J and Li L: Pterostilbene alleviates doxorubicin-induced cardiotoxicity by inhibiting cardiomyocytes pyroptosis mediated by the IL-6/STAT3-caspase-3/GSDME axis and M1 polarization of macrophages. Pharmacol Res 225: 108129, 2026.
43. Ajoolabady A, Pratico D, Mazidi M, Davies IG, Lip GYH, Seidah N, Libby P, Kroemer G and Ren J: PCSK9 in metabolism and diseases. Metabolism 163: 156064, 2025.
44. Shin D, Kim S, Lee H, Lee HC, Lee J, Park HW, Fukai M, Choi E, Choi S, Koo BJ, *et al*: PCSK9 stimulates Syk, PKCδ, and NF-κB, leading to atherosclerosis progression independently of LDL receptor. Nat Commun 15: 2789, 2024.
45. Bao H, Wang X, Zhou H, Zhou W, Liao F, Wei F, Yang S, Luo Z and Li W: PCSK9 regulates myofibroblast transformation through the JAK2/STAT3 pathway to regulate fibrosis after myocardial infarction. Biochem Pharmacol 220: 115996, 2024.
46. Liu Y, Zhao Y, Feng P and Jiang H: PCSK9 inhibitor attenuates atherosclerosis by regulating SNHG16/EZH2/TRAF5-mediated VSMC proliferation, migration, and foam cell formation. Cell Biol Int 47: 1267-1280, 2023.
47. Li ZZ, Guo L, An YL, Yu WJ, Shi DY, Lin QY and Zhang B: Evolocumab attenuates myocardial ischemia/reperfusion injury by blocking PCSK9/LIAS-mediated cuproptosis of cardiomyocytes. Basic Res Cardiol 120: 301-320, 2025.
48. Chung CC, Kao YH, Chen YC, Lin YK, Higa S, Hsu KC and Chen YJ: PCSK9 enhances cardiac fibrogenesis via the activation of Toll-like receptor and NLRP3 inflammasome signaling. Int J Mol Sci 26: 1921, 2025.
49. Huang Q, Zhou Z, Xu L, Zhan P and Huang G: PCSK9 inhibitor attenuates cardiac fibrosis in reperfusion injury rat by suppressing inflammatory response and TGF-β1/Smad3 pathway. Biochem Pharmacol 230: 116563, 2024.
50. Steffens D, Bramlage P, Scheeff C, Kasner M, Hassanein A, Friebel J and Rauch-Kröhnert U: PCSK9 inhibitors and cardiovascular outcomes. Expert Opin Biol Ther 20: 35-47, 2020.